UNIVERSIDADE FEDERAL DO PARANÁ

ANDREI CHADANOWICZ

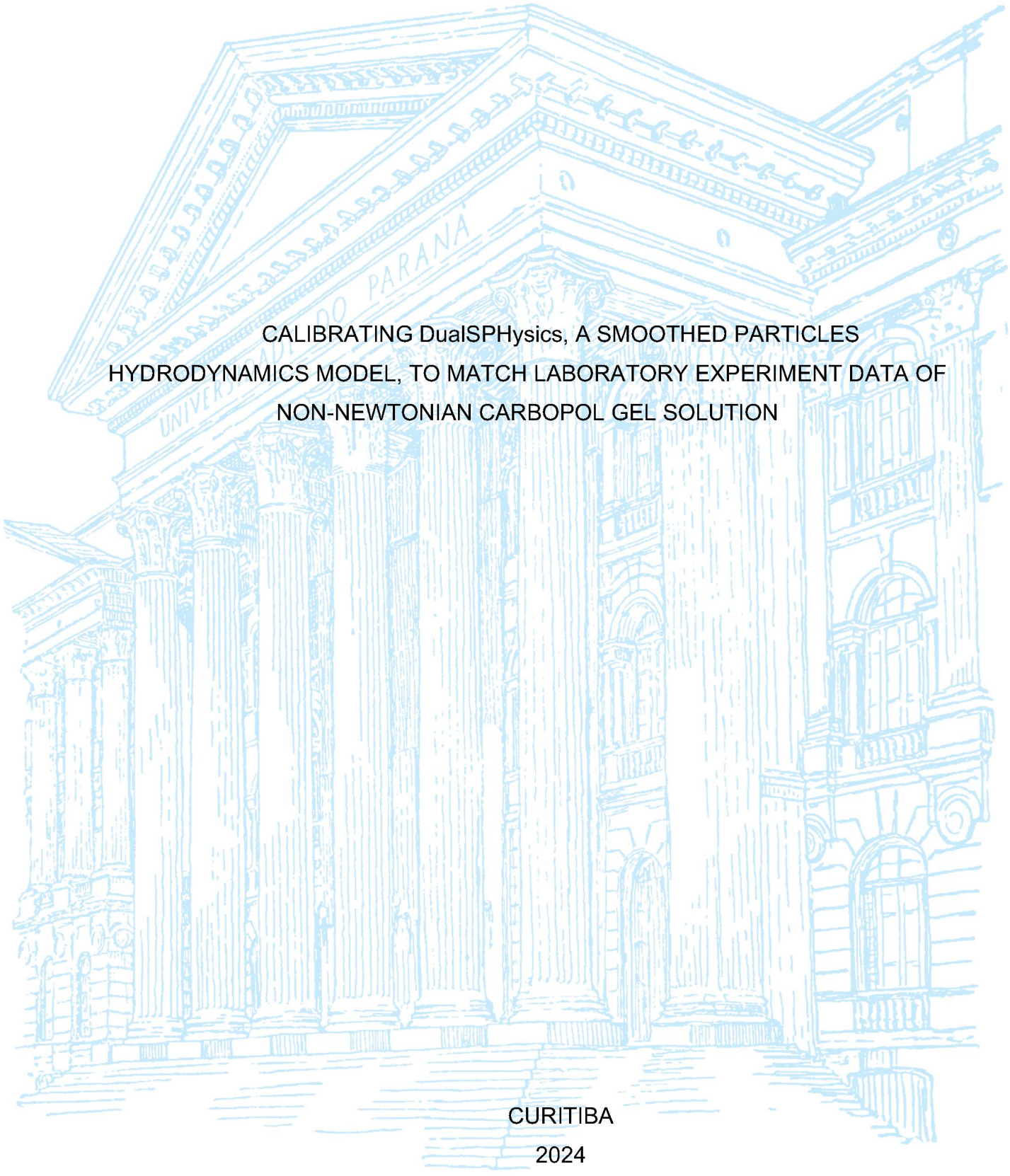

CALIBRATING DualSPHysics, A SMOOTHED PARTICLES HYDRODYNAMICS MODEL, TO MATCH LABORATORY EXPERIMENT DATA OF NON-NEWTONIAN CARBOPOL GEL SOLUTION

CURITIBA

2024

ANDREI CHADANOWICZ

CALIBRATING DUALSPHYSICS, A SMOOTHED PARTICLES HYDRODYNAMICS MODEL, TO MATCH LABORATORY EXPERIMENT DATA OF NON-NEWTONIAN CARBOPOL GEL SOLUTION

Dissertação apresentada ao curso de Pós-Graduação em Engenharia Ambiental, Setor de Tecnologia, Universidade Federal do Paraná, como requisito parcial à obtenção do título de Mestre em Engenharia Ambiental.

Orientador: Prof. Dr. Tobias Bernward Bleninger

CURITIBA

2024

DADOS INTERNACIONAIS DE CATALOGAÇÃO NA PUBLICAÇÃO (CIP)
UNIVERSIDADE FEDERAL DO PARANÁ
SISTEMA DE BIBLIOTECAS – BIBLIOTECA DE CIÊNCIA E TECNOLOGIA

Chadanowicz, Andrei
Calibrating dualsphysics, a smoothed particles hydrodynamics model, to match laboratory experiment data of non-newtonian carbopol gel solution / Andrei Chadanowicz. – Curitiba, 2024.
1 recurso on-line : PDF.

Dissertação (Mestrado) - Universidade Federal do Paraná, Setor de Tecnologia, Programa de Pós-Graduação em Engenharia Ambiental.

Orientador: Tobias Bernward Bleninger

1. Calibração. 2. Fluidos não-newtonianos. 3. SPH (Smoothed Particle Hydrodynamics). I. Universidade Federal do Paraná. II. Programa de Pós-Graduação em Engenharia Ambiental. III. Bleninger, Tobias Bernward. IV . Título.

Bibliotecário: Leticia Priscila Azevedo de Sousa CRB-9/2029

TERMO DE APROVAÇÃO

Os membros da Banca Examinadora designada pelo Colegiado do Programa de Pós-Graduação ENGENHARIA AMBIENTAL da Universidade Federal do Paraná foram convocados para realizar a arguição da Dissertação de Mestrado de **ANDREI CHADANOWICZ** intitulada: **CALIBRATING DualSPHysics, A SMOOTHED PARTICLES HYDRODYNAMICS MODEL, TO MATCH LABORATORY EXPERIMENT DATA OF NON-NEWTONIAN CARBOPOL GEL SOLUTION**, que após terem inquirido o aluno e realizada a avaliação do trabalho, são de parecer pela sua APROVAÇÃO no rito de defesa.

A outorga do título de mestre está sujeita à homologação pelo colegiado, ao atendimento de todas as indicações e correções solicitadas pela banca e ao pleno atendimento das demandas regimentais do Programa de Pós-Graduação.

Curitiba, 26 de Abril de 2024.

Assinatura Eletrônica
29/04/2024 07:26:26.0
TOBIAS BERNWARD BLENINGER
Presidente da Banca Examinadora

Assinatura Eletrônica
29/04/2024 11:58:57.0
BRUNO VICTOR VEIGA
Avaliador Externo (UNIVERSIDADE FEDERAL DO PARANÁ - DEP. DE HIDRÁULICA)

Assinatura Eletrônica
29/04/2024 09:36:25.0
MAURÍCIO FELGA GOBBI
Avaliador Interno (UNIVERSIDADE FEDERAL DO PARANÁ)

AGRADECIMENTO

Durante todo esse processo de mestrado houve muitos momentos de dificuldade e de questionamento, mas a rede de apoio que tive me fez conseguir superar estes momentos e concluir o que me decidi a fazer.

Gostaria de agradecer a minha família: meus pais por tornarem possível minha dedicação exclusiva à minha formação acadêmica e pelo apoio incondicional; e aos meus irmãos, por dividirem comigo a dificuldade da vida acadêmica.

Aos professores, por me inspirar e me encantar com novos conhecimentos. Em especial ao meu orientador, Tobias Bleninger, por me apresentar novas oportunidades, guiar em momentos de indecisão e incentivar durante dificuldades.

Aos meus colegas do mestrado, que agora também são amigos: Maria, Nathan e Luana, compartilhamos das mesmas dificuldades e dividindo nossas experiencias fizemos o caminho árduo muito mais agradável de trilhar.

Aos amigos que fizeram cada momento que passamos juntos durante esses anos especial.

Ao meu psicólogo por me fazer perceber e aceitar que o que eu fiz foi sempre meu melhor.

Ao professor Geraldo e ao Yuri, que me permitiram utilizar os seus dados experimentais para minha pesquisa e contribuíram com críticas e sugestões.

À CAPES por financiar minha pesquisa e tornar possível minha trajetória no mestrado. O presente trabalho foi realizado com apoio da Coordenação de Aperfeiçoamento de Pessoal de Nível Superior - Brasil (CAPES) - Código de Financiamento 001.

Agradeço a todos que estiveram comigo ao longo destes anos e, de alguma forma, contribuíram com meu processo de mestrado.

Look myself in the mirror, I say we gon' win

Knock me down nine times but I get up 10. (Cardi B, 2018, Get up 10)

RESUMO

DualSPHysics é um programa que utiliza o método de Smoothed Particle Hydrodynamics (SPH) para modelar fluidos, discretizando o domínio do fluido em um número finito de partículas. Neste trabalho, é realizada a calibração das configurações do programa para simular um fluido não-newtoniano, uma categoria de fluido que exibe comportamento de deformação não linear, e trabalhando com uma simulação tridimensional e partículas de contorno que simulam uma barragem que ascende em velocidade constante. Ao ajustar um modelo reológico que descreve o comportamento de fluidos não-newtonianos e sistematicamente combinando diferentes configurações do modelo, almeja-se calibrar o modelo DualSPHysics e coincidir os resultados com os dados experimentais do evento de rompimento de barragem com gel de Carbopol. Cada configuração é avaliada calculando o erro relativo aos dados experimentais, e a melhor é determinada pelo menor erro relativo. Os resultados da simulação final divergem dos dados experimentais, pois a influência das partículas de contorno que constituem a barragem é significativa, especialmente durante os estágios iniciais da simulação.

Palavras-chave: DualSPHysics; SPH; não-newtoniano; fluido; calibração.

ABSTRACT

DualSPHysics is a software that employs the Smoothed Particle Hydrodynamics (SPH) method to model fluids by discretizing the fluid domain into a finite number of particles. In this work, we attempt to calibrate the software's settings to simulate a non-Newtonian fluid, a type of fluid that exhibits non-linear deformation behavior, while working with a three-dimensional simulation and boundary particles that simulate a steadily rising dam. By fitting a rheological model that describes the behavior of non-Newtonian fluids and systematically combining different settings, we aim to calibrate the DualSPHysics model to match experimental data from a Carbopol gel dam-break scenario. Each setting is compared by calculating the relative error to the experimental data, and the best fit is determined based on the lowest relative error. The final simulation results diverge from the experimental data since the dam's boundary particles' influence is significant during the early stages of the dam-break simulation.

Keywords: DualSPHysics; SPH; non-Newtonian; fluid; calibration.

SUMMARY

Adjusting DualSPHysics, a Smoothed Particles Hydrodynamics Model, to Match Laboratory Experiment Data of Non-Newtonian Carbopol Gel Solution

Andrei Chadanowicz[1]

[1] Universidade Federal do Paraná

Abstract

DualSPHysics is a software that employs the Smoothed Particle Hydrodynamics (SPH) method to model fluids by discretizing the fluid domain into a finite number of particles. In this work, we attempt to calibrate the software's settings to simulate a non-Newtonian flow, a type of fluid that exhibits non-linear deformation behavior, while working with a three-dimensional simulation and boundary particles that simulate a steadily rising dam. By fitting a rheological model that describes the behavior of non-Newtonian fluids and systematically combining different settings, we aim to adjust the DualSPHysics model to match experimental data from a Carbopol gel dam-break scenario. Each setting is compared by calculating the relative error to the experimental data, and the best fit is determined based on the lowest relative error. The final simulation results diverge from the experimental data since the dam's boundary particles' influence is significant during the early stages of the dam-break simulation.

1 INTRODUCTION

As the global population continues to grow, the demand for resources and living spaces escalates accordingly. One critical aspect of resource extraction involves mining facilities, which employ dams to contain the waste generated during the extraction process. This waste material, known as tailings, is composed primarily of fine grains, such as clay, silt and fine sand (Hu et al. 2017; Jing et al. 2019). Tailings are generally transported in liquefied form to the tailing dams through pipeline systems (Boger

Corresponding author(s): Andrei Chadanowicz, Universidade Federal do Paraná, andreichadanowicz@ufpr.br

2013). However, the rheological nature of liquefied mining tailings deviates from the behavior of Newtonian fluids, such as water and oil, being considered a non-Newtonian fluid (O'Brien et al. 1993; Moon et al. 2019). The study of rheological properties of tailings and their flow plays a vital role in establishing safety protocols and in determining flooded areas for mining waste dams through a tailings dambreak analysis (de Paiva et al. 2020). This analysis is usually carried out with numerical codes, which require rheological properties of the flowing material as input parameters. Thus, by investigating the rheological properties of these materials, researchers can establish effective measures to ensure the safety of people living around mining waste dams.

Nevertheless, the study of non-Newtonian fluid flows is a non-trivial challenge, since non-Newtonian rheological models are often more complex than the standard Newtonian model. If the classical Newtonian fluid mechanics theory provides only a few analytical solutions, the non-Newtonian theory provides even less. With the advance of computational power, Computational Fluid Dynamics (CFD) poses itself as a field that facilitates the study of non-Newtonian flows by simulating the behavior of fluids through computational means. By applying numerical methods and algorithms, CFD offers a powerful tool to model and analyze the intricate dynamics of fluids, including the non-Newtonian fluids.

When simulating non-Newtonian fluids, computational dynamics software frequently rely on either the finite difference method or the finite volume method to solve the governing differential equations, that ensures a balance of flux, mass, and momentum across the boundaries of discretized control volumes. Noteworthy software used for non-Newtonian fluid simulation includes, for instance, FLO-2D/3D, HEC-RAS, Riverflow2D, DHI MIKE 21/3, FLOW3D, and DAN3D (Liu & Henderson 2020).

Within the domain of CFD, Smoothed Particle Hydrodynamics (SPH) has emerged as a paradigm-shifting approach. In contrast to conventional grid-based methods, SPH employs a particle-based framework fit to simulate problems with a complex frontier dynamic. The fundamental principle of SPH revolves around discretising the fluid domain into discrete particles, each with properties like mass, position, and velocity. Interactions between pairs of particles inside smoothing kernels are calculated using hydrodynamics equations that dictate fluid behaviours.

One of the key advantages of SPH lies in its ability to handle fluid flows with high deformability, complex boundaries and free surfaces (Desbrun & Gascuel 1996), meanwhile, the treatment of boundary conditions is certainly one of the difficult technical points of the method. The particle-based nature of SPH allows for easier free surface fluid scenarios and handling of multiphase interactions (Hu & Adams 2006), making

it well-suited for simulating scenarios such as liquid sloshing (Shao et al. 2012), dam break simulations, and ocean waves (Dalrymple & Rogers 2006). It also works well with complex and moving boundaries, which are notably difficult to simulate using mesh-based simulations (Crespo et al. 2007).

.

1.1 OBJECTIVES

The primary objective of this work is to present the application of the DualSPHysics model in simulating a case of idealized dam break scenario of a non-Newtonian fluid: carbopol gel. We aim to bridge the gap between experimental observations and computational simulations by comparing the simulated results obtained through SPH with avaiable experimental data.

DualSPHysics was already used in similar fashion to simulate classic dambreak scenarios of non-newtonian fluids and compare to experimental data. (Shao & Lo 2003) did a work with non-Newtonian SPH and dambreak real-life experiments while using an incompressible SPH formulation and achieved good agreement between numerical simulations and available experimental data. Hosseini et al. (2007) also worked with non-Newtonian SPH simulations and used a weakly-compressible formulation to achieve numerical results that closely agrees with experimental data. These studies exemplify the effectiveness of SPH in capturing the complexities of non-Newtonian fluid dynamics during dam-break events.

Both of the previously mentioned articles worked with two dimensional simulations of instantaneously released fluid. Here, we work with a three dimensional simulation, but take into account the speed at which the dam rises to mirror experimental conditions. These could prove to be big influences on the way the fluid behaves throughout the simulations.

2 INTRODUCTION TO RHEOLOCIAL ASPECTS

Rheology can be understood as the science that study the deformation and flow of materials. In order to characterize rheologically a material, a relationship between shear stress (τ) and shear rate ($\dot{\gamma}$) is required, producing the flow curve. Several experimental techniques are used to determine the flow curve by exerting a known shear stress and measuring the shear rate, or vice-versa. Then, a rheological model is adjusted to the flow curve points and the corresponding rheological parameters are obtained. The simplest, one dimensional, model is the Newtonian model (equation 1),

featuring a linear relationship between shear rate (τ) and shear stress, usually denoted as the partial derivative of velocity with respect to a perpendicular direction ($\dot{\gamma}$), and connected by dynamic viscosity (μ).

$$\tau = \mu \, \dot{\gamma} \tag{1}$$

Other rheological models are capable of modelling further properties. The power-law model, for example:

$$\tau(\dot{\gamma}) = K_n(\dot{\gamma})^n \tag{2}$$

is able to model shear-thinning or thickening properties, where the shear stress is not directly proportional to the shear rate. Shear-thinning fluids, also known as pseudoplastic fluids ($n < 1$), such as certain polymer solutions, display a decrease in apparent viscosity as the applied shear rate increases. On the other hand, shear-thickening fluids, also known as dilatant fluids ($n > 1$), such as suspensions of cornstarch in water, exhibit an increase in apparent viscosity with increasing shear rate. The Newtonian model is recovered if $n = 1$. In this model, the dynamic viscosity is replaced by the consistency (K_n).

In the context of liquefied mining tailings, these materials are commonly described as viscoplastic fluids, or yield stress fluids (Kwak et al. 2005). They require a certain amount of stress, known as the yield stress (τ_c), to start deforming. For an applied shear stress below the yield stress, the fluid behaves as a solid material, resisting deformation. Once the yield stress is overcome , flow starts, and the fluid exhibits liquid behavior . A more general rheological model, the Herschel-Bulkley model (Herschel & Bulkley 1926), captures both shear-thinning (or dilatancy) and viscoplasticity, as shown in Equation 3:

$$\begin{cases} \tau(\dot{\gamma}) = \tau_c + K_n\dot{\gamma}^n & if \ \tau \geq \tau_c \\ \dot{\gamma} = 0 & if \tau < \tau_c \end{cases} \tag{3}$$

with the shear stress represented as $\dot{\gamma}$. If $\tau_c \neq 0$ and $n = 1$, the Bingham model is obtained, which is commonly employed to describe liquefied tailings (Boger 2013).

The application of rheological models in CFD relies on including them at the viscous term of the governing momentum equations. Equation 4 shows the Herschel-Bulkley model in terms of apparent viscosity η, by dividing Equation 3 by $\dot{\gamma}$:

$$\eta(\dot{\gamma}) = \frac{\tau_c}{\dot{\gamma}} + K_n\dot{\gamma}^{n-1} \tag{4}$$

If the shear rate tends to zero, i.e. regions where the flow is almost uniform, the apparent viscosity tends to infinity. This creates numerical instabilities in numerical simulations. Thus, regularization models are used to circumvent this challenge, with different methods being employed in the literature, such as the Herschel-Bulkley-Papanastasiou model (equation 5 below) (Papanastasiou 1987) and bi-viscosity models (Frigaard & Nouar 2005).

$$\eta(\dot{\gamma}) = \frac{\tau_c}{\dot{\gamma}}[1 - \exp(-m\dot{\gamma})] + K\eta^{n-1} \tag{5}$$

With the equation above having the same variables as equation 4, but with an added exponential term with a calibration parameter m to account for the discontinuity. As the argument of the exponential increases, this term will approach zero and the model should behave the same as the Herschel-Bulkley model in equation 4.

In this study a Bingham model is employed with a regularization parameter B to tune the yield region and keep the apparent viscosity from becoming too high:

$$\begin{cases} \eta(\dot{\gamma}) = K(B+1) & if\ \dot{\gamma} < \tau_c/2KB \\ \eta(\dot{\gamma}) = \frac{\tau_c}{\dot{\gamma}} + K\dot{\gamma}^{n-1} & if\ \dot{\gamma} \geq \tau_c/2KB \end{cases} \tag{6}$$

This equation keeps the behavior of the fluid consistent with the Herschel-Bulkley model for higher strain rates and prevents the apparent viscosity from reaching high numbers at lower strain rates.

3 SPH BACKGROUND AND FORMULATION

The Smoothed Particle Hydrodynamics (SPH) method was originally introduced by Gingold & Monaghan in 1977 as a computational technique for simulating astronomical phenomena. It's formulated (equation 7) as the convolution of a function $f(x')$ and a kernel function, $W(x,h)$, with h being the smoothing length of the kernel function, on a point x over an Ω domain. The kernel function plays a crucial role in SPH by approximating the behavior of a Dirac delta function, facilitating the smooth spread of properties and interactions between neighboring particles.

$$f(x) \approx \int_{\Omega} f\,(x')\, W(x - x',\ h)dx' \tag{7}$$

Upon employing the equation (7) across the spatial domain, where f denotes a property of interest within the domain, the continuous medium undergoes a process of discretization. In this discretized representation, the continuous domain is subdivided

into individual particles. Each particle represents specific attributes of the underlying continuous domain in a discrete form. This discretization process allows us to transition from a continuum representation to a particle-based representation. Once this transition is made, the properties of each particle need to be updated throughout the simulation and the interactions between particles must be calculated. To achieve this, we discretize the equation into a finite form:

$$\langle f(x) \rangle \approx \sum_{j}^{N} f\left(x_j\right) W(x - x_j,\ h) V_j \tag{8}$$

taking into account all neighboring particles (j) within the smoothing length of the kernel and their pairwise interaction with the particle to be updated (i). By considering these neighbouring particles, we can accurately update the properties defined by the function $f(x)$ and account for the influences of nearby particles. A visual representation of the updated particle and the support kernel containing the neighbouring particles that influence each update is in figure 1.

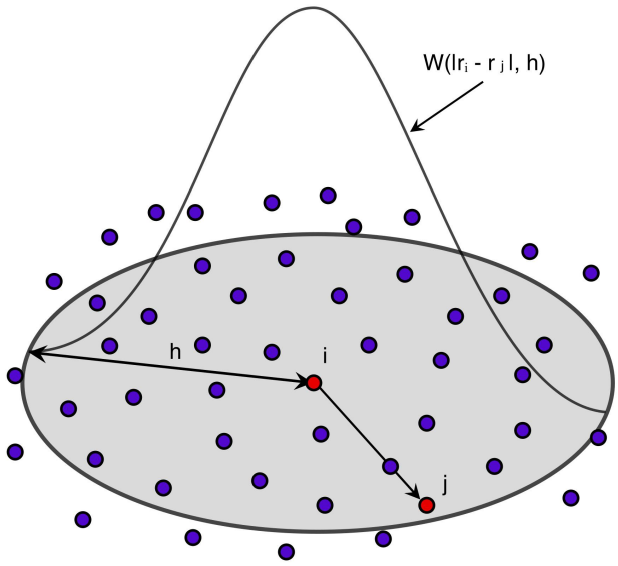

Figure 1: SPH particles and Smoothing Kernel Representation

By making i our interpolation particle and j the support particles, writing $W(x - x_j,\ h)$ as W_{ij} meaning the value of the kernel function between the two particles and considering the volume V_j as the ratio between the mass m_j and the density ρ_j of the

particle j, we can rewrite the SPH interpolation as:

$$\langle f(x_i)\rangle = \sum_{j}^{N} \frac{m_j}{\rho_j} f_j W_{ij} \tag{9}$$

In order to emulate the functionality of the Dirac delta function, the smoothing kernel employed in SPH simulations must adhere to specific conditions. Firstly, like the Dirac delta function, the integral of the kernel function over the domain must equal one. This ensures that the integral of the kernel remains bounded between zero and one, preserving the conservation properties of the simulation. Additionally, the kernel function must exhibit sufficient smoothness to allow the computation of derivatives (Monaghan & Lattanzio 1985).

As we study fluid dynamics, we need to use the SPH discretization on key equations that govern fluid behaviours. These equations include the Cauchy momentum equation and the continuity equation. With these equations we aim to solve and find velocity, pressure and density. With three variables to solve for and two equations, there is a need for a closing equation. The one implemented in DualSPHysics was proposed by Monaghan et al. (1999) as a closing equation for SPH models.

4 METHODOLOGY

The SPH DualSPHysics model was employed to simulate a scenario akin to experiments conducted on non-Newtonian Carbopol gel by São (2021). Various configurations of the DualSPHysics model were evaluated to determine the optimal setup for achieving accuracy in comparison to experimental data.

While applying the DualSPHysics model, its effectiveness hinges not only on choosing the right parameters but also ensuring its fine-tuning through calibration. This relationship between parameter sensitivity and model fit determines the accuracy with which the simulation mirrors experimental data. In this study, we delve into the process of calibration, aiming to optimize parameters and elevate the model's fidelity to real-world observations.

However, not all settings prove equally effective. Through this work, we identify and separate configurations that do not yield satisfactory results. This preliminary step is crucial before comparing various combinations of settings that result in more subtle differences between each other, ensuring a more concise analysis. The configurations tested and compared in this work are shown in the flowchart (Figure 2), the ones that were shown to be worse are not carried through to the final scenarios tested.

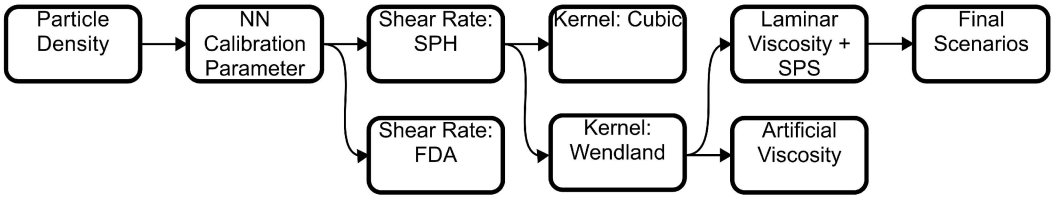

Figure 2: Flowchart of the Scenarios Simulated Throughout this work

Our initial simulations utilized a specific configuration chosen for its proximity to the final, optimized setup presented later in this article. This setup employed a Verlet time step, Wendland smoothing kernel, Laminar and sub-particle turbulence approximation viscosity treatment, Fourtakas particle shifting, and the SPH method for calculating fluid shear strain. This selection offered a starting point for assessing the sensitivity of our results to other settings and understanding their influence on deviation from expected, experimentally validated outcomes.

4.1 EXPERIMENTAL SCENARIO

Sáo (2021) set up a typical dambreak experiment using Carbopol gel and a camera to record how the fluid flows (figure 3). The rising dam was set to rise at a steady rate to keep the velocity constant. The fluid's reach was taken from the images recorded with the camera and applying the Canny Edge Detector algorithm (Ding & Goshtasby 2001). Data compared was from a scenario with rising dam speed of 0.17 m/s. Two distance sensor were also mounted on top of the experiment to measure the fluid depth. One sensor 615 mm from the back of the tank and the second 725 mm from the back. Initial setup parameters scheme can be seen in figure 4.

Figure 3: Experimental Tank Initial Setup For Data Recording from Sáo (2021)

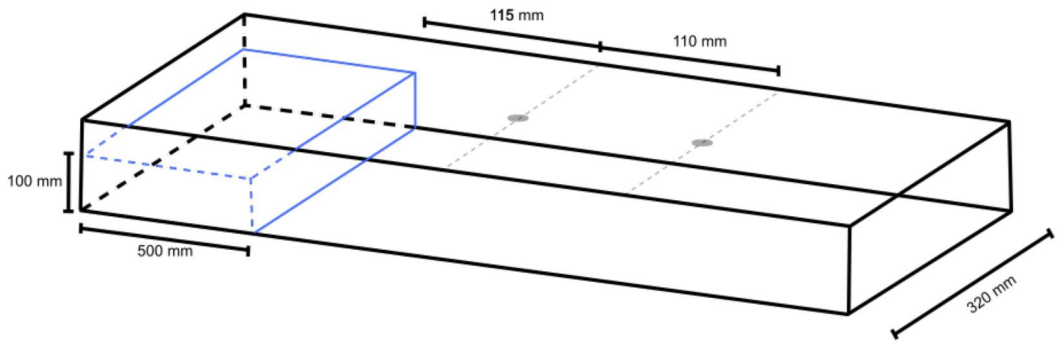

Figure 4: Experiment and Simulation Starting Configuration and Dimensions

The fluid's rheological properties were defined by Pereira (2018) using a rheometer and determining Herschel-Bulkley coefficients: shear yield stress (τ_c), consistency (K_n) and flow index (n). A gel solution of Carbopol 996 polymer with 0.17% mass was used. Its adjusted properties are: density of 1000kg/m^3 and rheological properties: 57.12 Pa shear yield stress, 15.35Pa.s^n consistency and 0.420 flow index.

The non-Newtonian characteristics and parameters were incorporated into the DualSPHysics model. Meanwhile, the experimental geometry served as the model's initial condition, providing a foundation for attempting to replicate the observed results.

4.2 DUALSPHYSICS

This work was realised using the open-source DualSPHysics model (Domínguez et al. 2021), which uses both the computer's CPU and GPU for processing, making it more efficient and faster than a regular CPU implementation due to the architecture difference. The GPU implementation of SPH via CUDA benefits from the inherent centered and explicit nature of the formulation (Crespo et al. 2011).

CUDA serves as a powerful programming platform facilitating the utilization of a computer's Graphics Processing Unit (GPU) for general-purpose computing. Harnessing the distinctive architecture of GPUs, it enables superior computing performance in tasks demanding a high level of parallelization. This stands in contrast to computations executed solely by the computer's Central Processing Unit (CPU), as the GPU's architecture excels in parallel processing (Owens et al. 2008).

With this approach, the properties of each particle can be updated independently during each time step. This characteristic allows for efficient parallelization, enabling the simultaneous update of multiple particles as long as there is sufficient computa-

tional power available. By harnessing the capabilities of GPU processing, the SPH implementation becomes highly optimized, enhancing the speed and efficiency of the simulation (Hérault et al. 2010).

The model setup steps are outlined in the following flowchart (Figure 5). It's important to note the sequence of setup steps, as the initial and boundary conditions depend on the smoothing length due to the potential gap formation between boundaries and fluid particles, which is further explained later. Post-processing is configured separately in DualSPHysics, as desired variables need to be calculated using the SPH summation formula (equation 8) for each desired position that isn't occupied by a particle.

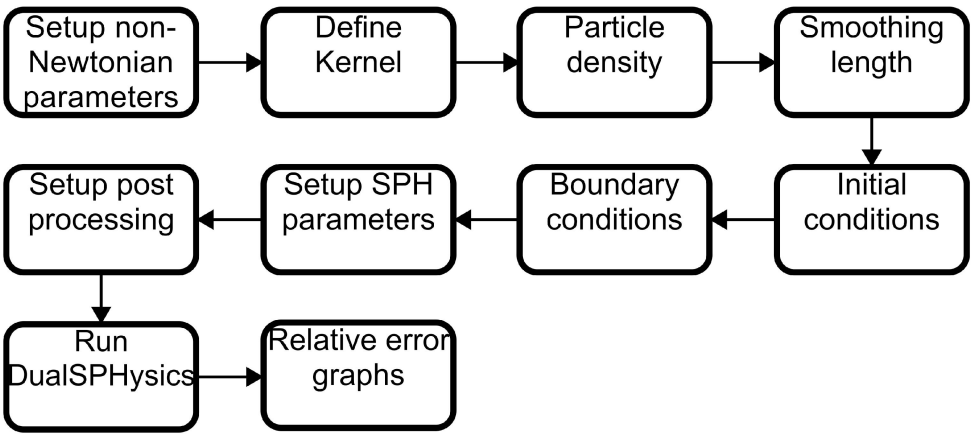

Figure 5: Flowchart of the Setup Steps used for running DualSPHysics model

4.3 INITIAL AND BOUNDARY CONDITIONS

As mentioned earlier, the initial conditions for the SPH model are configured based on the experiment's geometry. The conversion of the experiment's physical components, including walls and the fluid, into discrete particles is achieved by implementing SPH equations with an internal particle distance set at 0.004 m. The boundary particles and rising dam can be seen in figure 6.

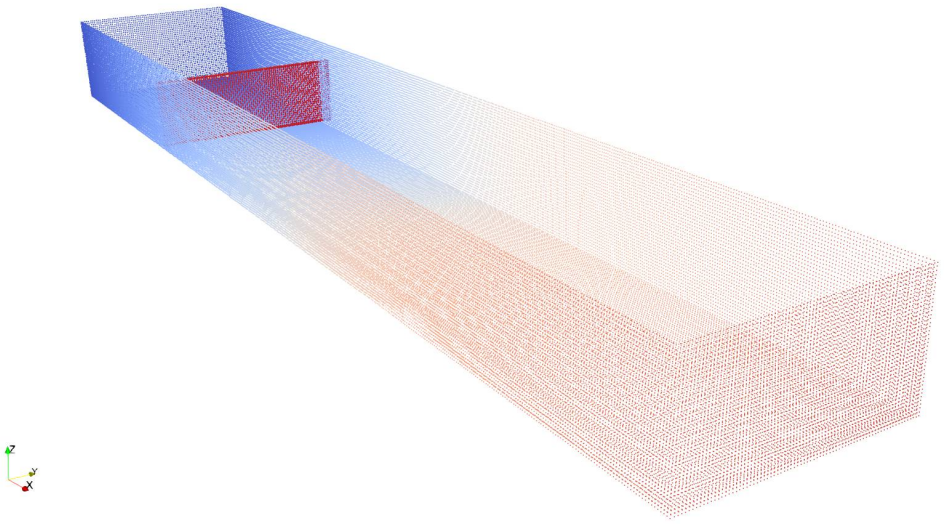

Figure 6: Boundary Particles Used on the SPH Simulations

Boundary conditions in the SPH model are established by configuring particles that remain stationary. However, these stationary particles undergo updates in their density throughout the simulation, mirroring the behavior of other SPH particles (Crespo et al. 2007). This continual adjustment in density, proposed by Dalrymple & Knio (2001), serves as a mechanism that prevents particles from breaching the simulation borders, as opposed to a simple no-slip condition.

In order to simulate the ascending dam, a specific set of boundary particles constituting the dam are given a consistent upward velocity of 0.17 m/s. Different from the stationary particles used in typical boundary conditions, these particles possess a fixed non-zero speed.

4.4 RESOLUTION AND PARTICLE DENSITY

When employing SPH, there's no need for a mesh grid that must be refined locally and tailored to the desired domain. Also, unlike traditional numerical methods like finite differences, SPH doesn't follow the same convergence conditions. Therefore, determining the resolution must be approached differently.

What is commonly employed to determine the particle density in SPH simulations is doubling the number of particles modelled until the results converge between two simulations (Lo & Shao 2002; Fang et al. 2022). This way ensures the particle number is no longer affecting the simulation by means of lack of particles or by a saturation of particles inside the smoothing length (Quinlan et al. 2006).

The resolution employed in this work was of 0.004m between each particle, result-

ing in a total of 305,077 particles. While this resolution fits the previously mentioned criteria (half of this resolution wields the same results), it was chosen as to use all the computational power available, as our used machine couldn't handle higher resolutions.

The computer used for the simulations had an Intel i5 10th generation processor (model i5-10400F) with 16 gigabytes of avaiable RAM and a NVIDIA GeForce GTX1650 with 4 gigabytes of dedicated GPU memory that was used for the simulations.

4.5 BI-VISCOUS CALIBRATION PARAMETER

As mentioned earlier, the utilization of the bi-viscous formula involves a calibration parameter. To determine the optimal value for this parameter, a series of simulations were conducted, each employing different values for the calibration parameter. The average relative error was calculated for each calibration parameter simulation in order to find the lowest relative error. The objective was to discern which parameter value would most closely simulate the previous experimental outcomes.

The outcomes of these simulations are visually represented in figure 7. The best fit was chosen based on the lower average relative error in relation to the experimental data, the values for the average relative error are shown in figure 8. The value of B=0.005 exhibits a commendable level of agreement with the lowest average relative error of the other simulations of 10%. However, it is imperative to note that, particularly during the initial phases of the flow, the simulation does not entirely align with the experimental data.

$$\begin{cases} \eta(\dot{\gamma}) = K(B+1) & if\ \dot{\gamma} < \tau_c/2KB \\ \eta(\dot{\gamma}) = \frac{\tau_c}{\dot{\gamma}} + K\dot{\gamma}^{n-1} & if\ \dot{\gamma} \geq \tau_c/2KB \end{cases} \tag{10}$$

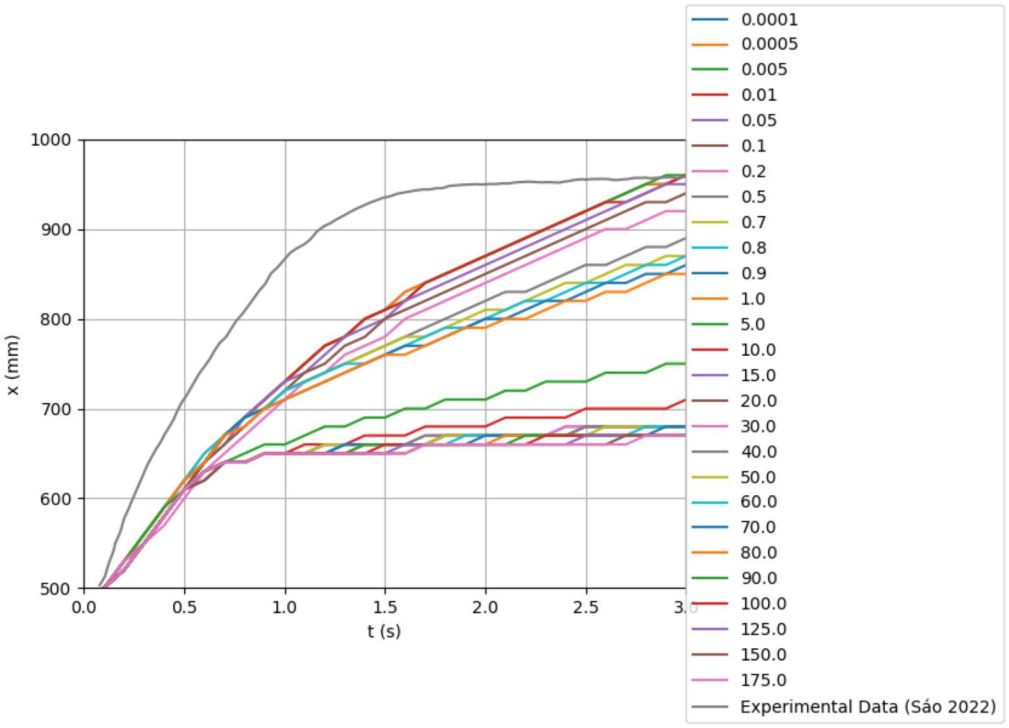

Figure 7: Simulation Results for each Tested non-Newtonian Calibration Parameter

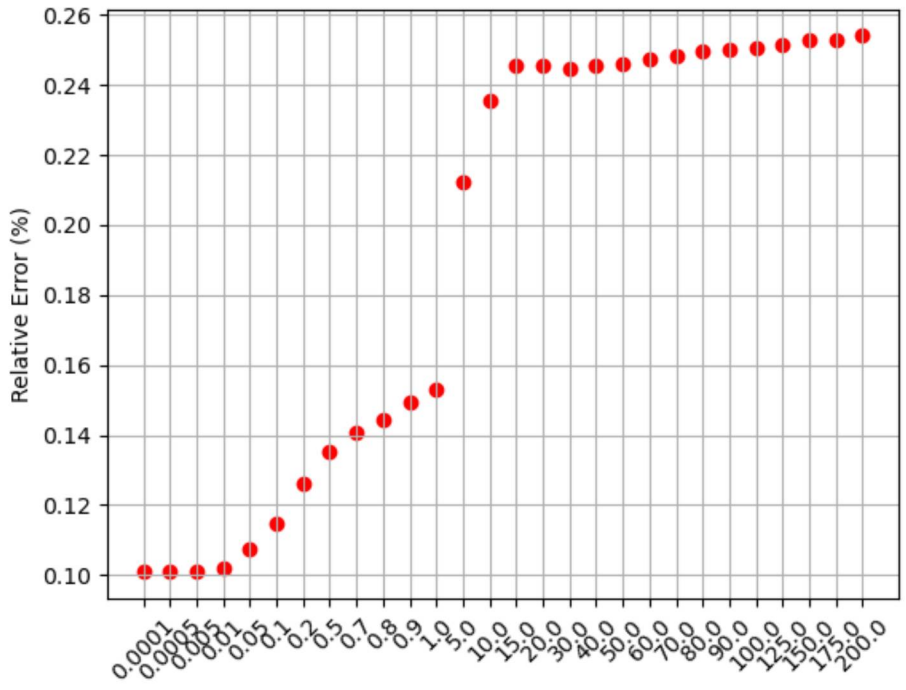

Figure 8: Average Relative Error for Each Tested Calibration Parameter

4.6 SHEAR RATE CALCULATION

In DualSPHysics, shear rate can be calculated through two different ways. The first employs the conventional Smoothed Particle Hydrodynamics (SPH) formulation to obtain velocity derivatives. The second method involves an adaptation of Finite Differences (FDA), determined by the difference between the velocity of a particle and that of its neighboring particles.

4.6.1 SPH Calculation for Shear Rate

A fundamental expression for calculating the derivative of a function within Smoothed Particle Hydrodynamics, as demonstrated by Monaghan (1982), is given by:

$$\langle \nabla f(x_i) \rangle = \sum_{j}^{N} \frac{m_j}{\rho_j} (f_j - f_i) \nabla_i W_{ij} \tag{11}$$

Here, ∇f represents the derivative of the function, and ∇W signifies the derivative of the smoothing kernel. This formulation allows us to obtain derivatives by utilizing solely the derivative of the kernel. In the context of calculating shear rate, velocity is employed to determine the rate concerning the direction perpendicular to the line connecting the particles.

The outcomes of the simulation utilizing the SPH calculation for shear rate are depicted in Figures 9 and 10. Notably, these figures correspond to the identical settings employed in the earlier determination of parameter B.

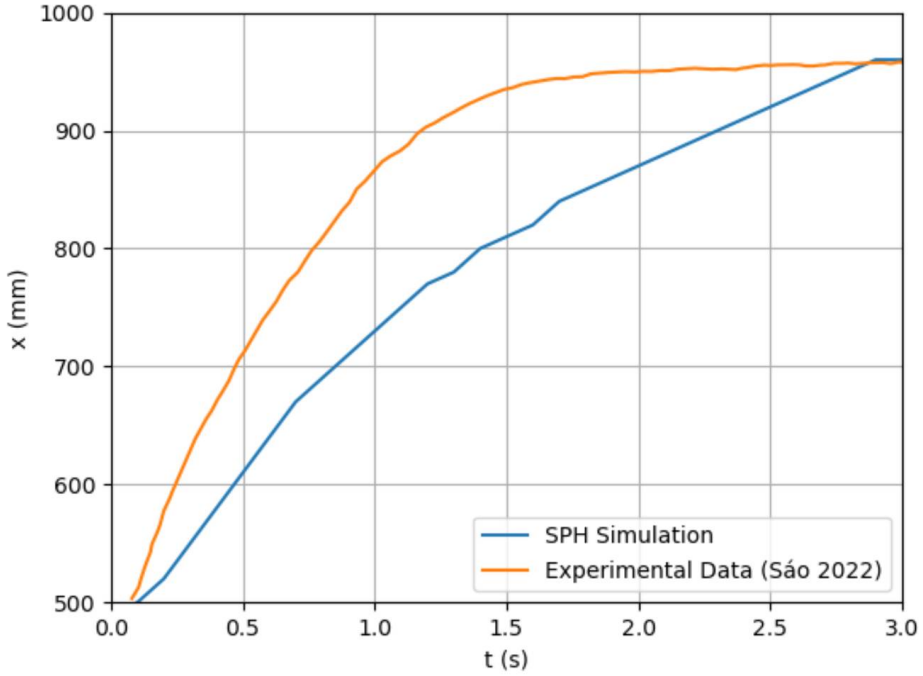

Figure 9: SPH Results for the Dambreak Wave Reach Throughout the Simulation Using SPH Shear Rate Calculation

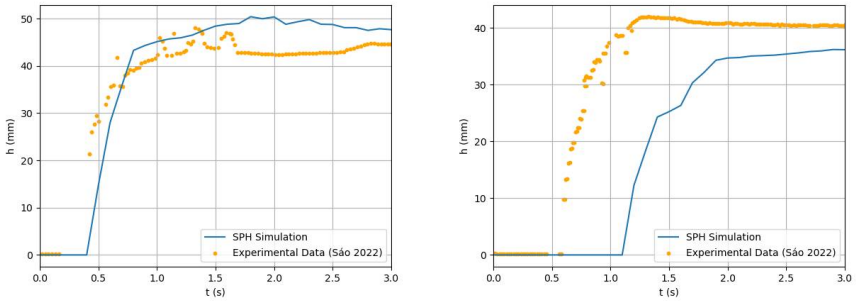

(a) Sensor1 (b) Sensor 2

Figure 10: SPH Results for Depth Below each Sensor Throughout the Simulation Using SPH Shear Rate Calculation

For comparison between both results, the relative error calculated for the simulation results are shown in figure 11. The average relative error for SPH calculation of the shear rate was of 10%. While the average relative error for both sensor 1 and 2 were 12% and 23%, respectively.

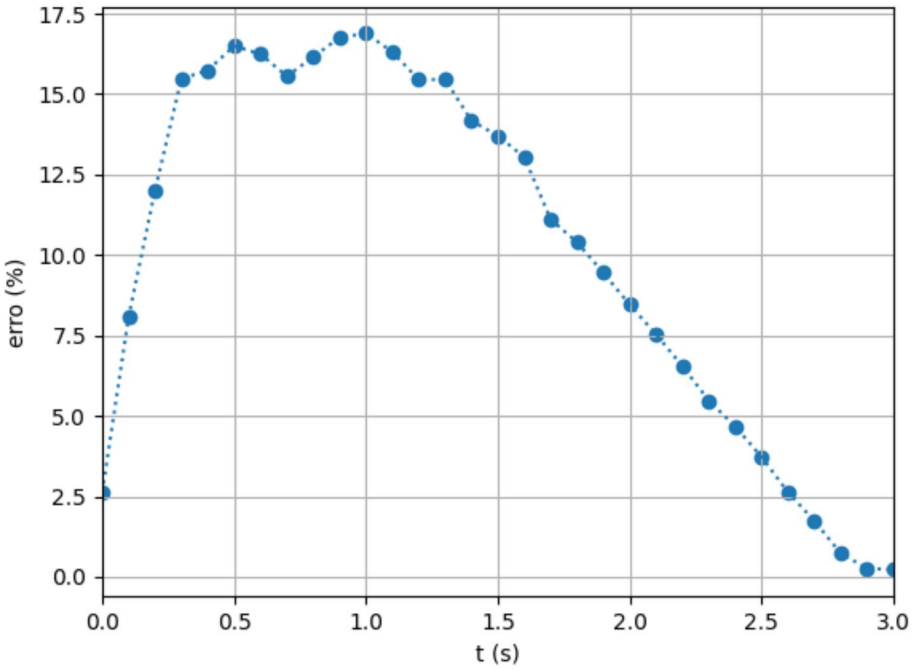

Figure 11: Relative Error Throughout the Simulation for SPH Calculation of the Shear Rate

4.6.2 FDA Calculation for Shear Rate

In contrast to the SPH formulation, the FDA method employs finite differences between particles to compute shear rate. This approach is comparatively simpler to implement than the SPH method.

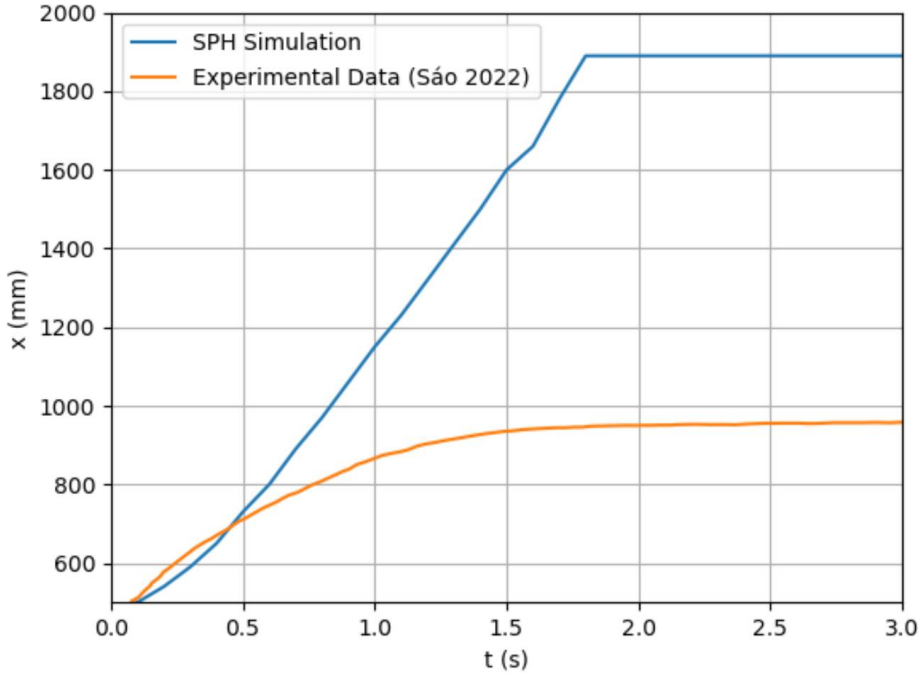

Figure 12: SPH Results for the Dambreak Wave Reach Throughout the Simulation Using FDA Shear Rate Calculation

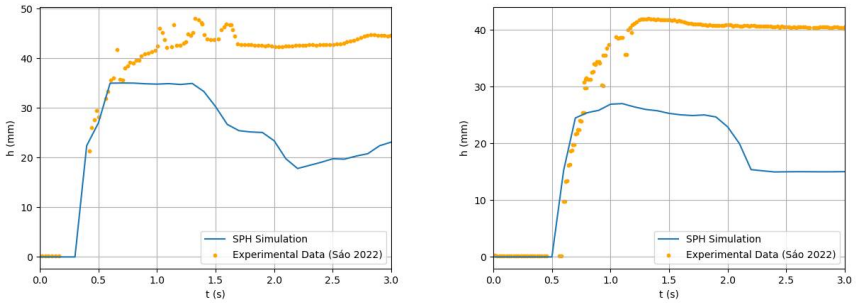

(a) Sensor1 (b) Sensor 2

Figure 13: SPH Results for Depth Below each Sensor Throughout the Simulation Using FDA Shear Rate Calculation

The relative errors for the FDA way of calculating shear rate were bigger than the relative errors for the SPH way (Figure 14), averaging 59% for the evolution of the flow's reach and; 36% and 44% for each sensor respectively, which are also bigger relative errors than the SPH method's.

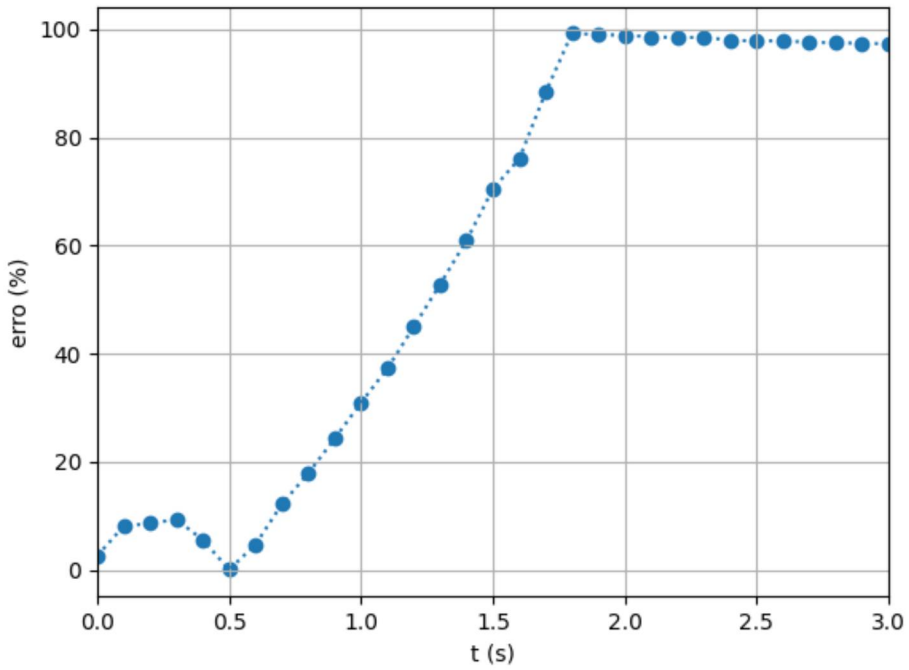

Figure 14: Relative Error Throughout the Simulation for FDA Calculation of the Shear Rate

It is evident that the FDA method failed to accurately capture the rheological characteristics of the fluid during the simulation. Consequently, the SPH formulation stands out as the superior choice.

4.7 KERNEL

Selecting the most suitable kernel is crucial for an effective simulation. Polynomial expressions are often favored for their computational efficiency. In our comparison, we evaluate the performance of both cubic and quintic formulations, the former being developed by Monaghan & Lattanzio and the latter by Wendland.

4.7.1 Cubic Spline

Monaghan & Lattanzio (1985) introduced a kernel cubic spline formulation expressed as:

$$W(r,h) = \alpha_D \begin{cases} 1 - \frac{3}{2}q^2 & if\ 0 \leq q \leq 1 \\ \frac{1}{4}(2-q)^3 & if\ 0 \leq q \leq 1 \\ 0 & if\ q \geq 2 \end{cases} \tag{12}$$

Here, the variable q denotes the distance between particles, and the coefficient α_D is set to $1/\pi h^3$ for the three-dimensional kernel. The simulation results are presented in Figures 15 and 16.

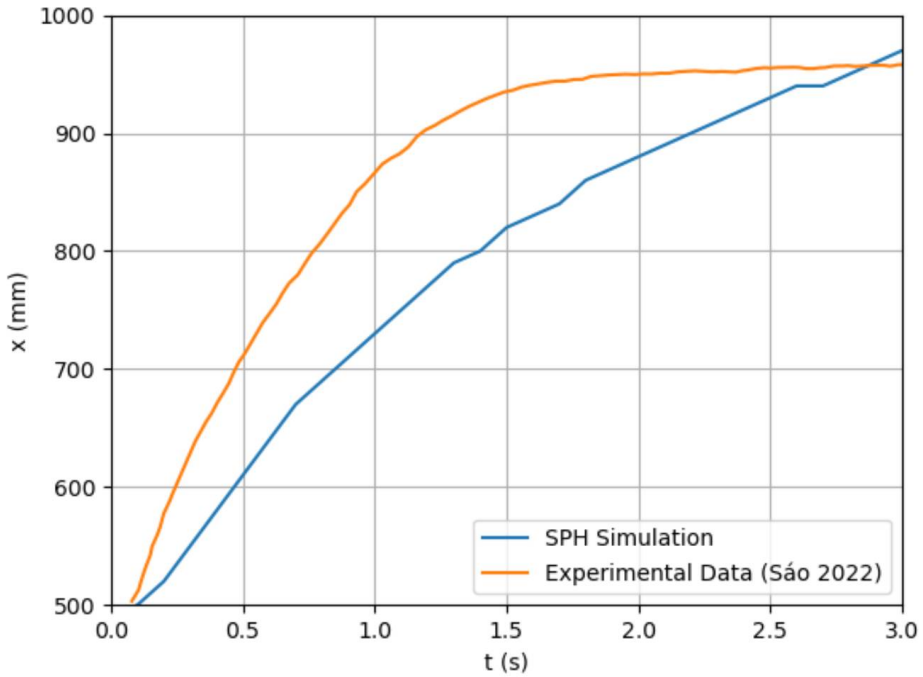

Figure 15: SPH Results for the Dambreak Wave Reach Throughout the Simulation Using Cubic Kernel

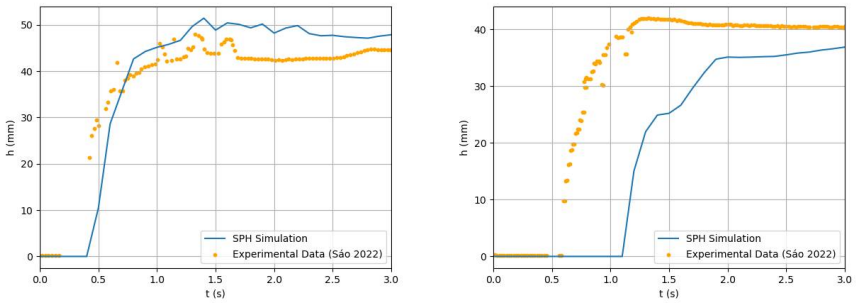

(a) Sensor1 (b) Sensor 2

Figure 16: SPH Results for Depth Below each Sensor Throughout the Simulation Using Cubic Kernel

Testing the relative errors throughout the simulation ran using the Cubic Spline Kernel (Figure 17) resulted in an average relative error of 10% for the wave's reach. Meanwhile the average relative errors of the fluid depth below the sensors were 13% and 22% respectively.

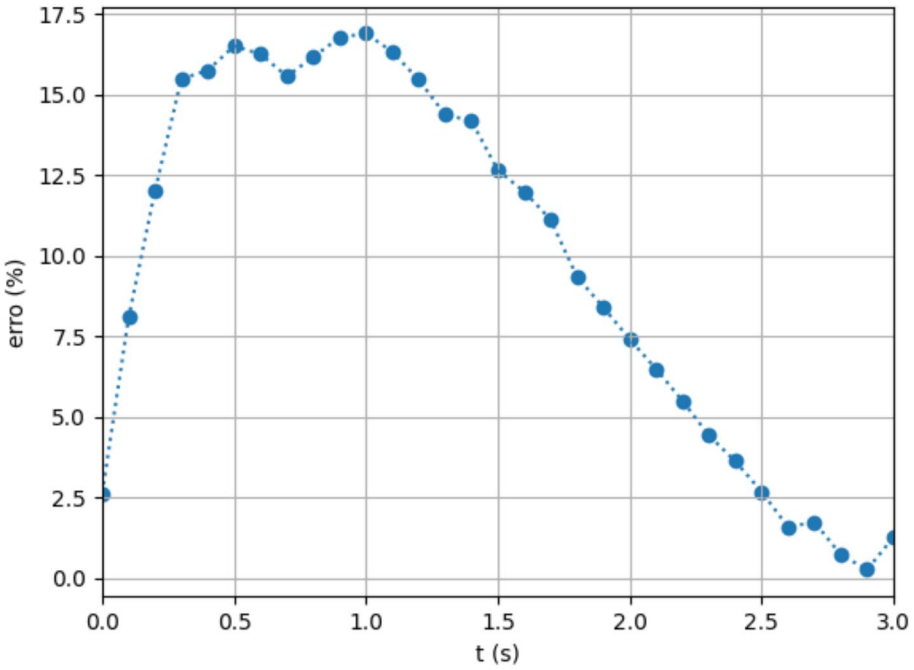

Figure 17: Relative Error Throughout the Simulation for the Cubic Spline Kernel

4.7.2 Wendland

In this case, the smoothing kernel employed is a quintic equation developed by Wendland (1995):

$$W(r,h) = \alpha_D \left(1 - \frac{q}{2}\right)^4 (2q+1), \quad \text{with } 0 \leq q \leq 2 \tag{13}$$

where q represents the distance between two particles and the coefficient α_D is set to $21/16\pi h^3$ for the three-dimensional kernel. This also being a polynomial equation means it will also benefit from reduced run times.

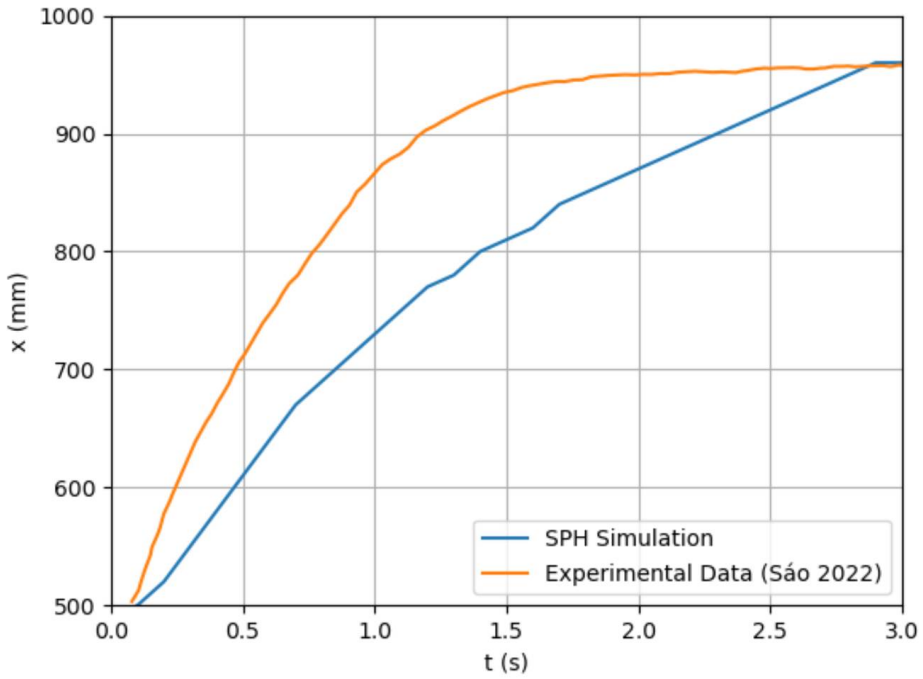

Figure 18: SPH Results for the Dambreak Wave Reach Throughout the Simulation Using wendland Kernel

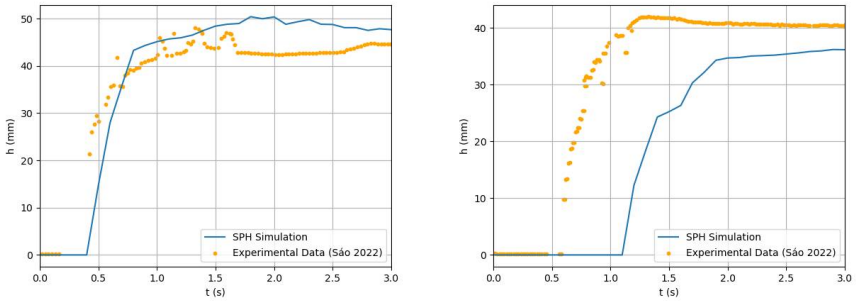

(a) Sensor1 (b) Sensor 2

Figure 19: SPH Results for Depth Below each Sensor Throughout the Simulation Using Wendland Kernel

The relative error calculated for the simulation results using the Wendland kernel are shown in Figure 20. The average relative error was 10% for the reach and 12% and 23% for each sensor.

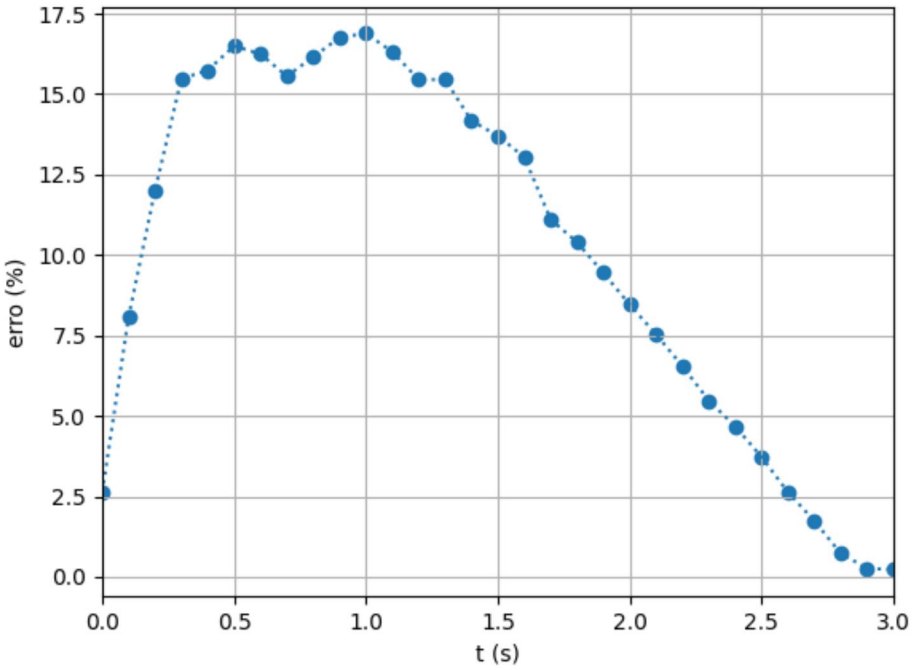

Figure 20: Relative Error Throughout the Simulation for the Wendland Spline Kernel

Upon comparing the results, it's not obvious which kernel formulation performed better than the other. The differences in average relative error are also very small, being Cubic Spline better by 1% on the first sensor and the Wendland kernel better by 1% also on the second sensor's results. The Wendland kernel was chosen, in the end, because it's simulation did not go over the maximum reach measured experimentally, while the Cubic Spline results' did.

4.8 ARTIFICIAL VISCOSITY

Artificial viscosity serves as a crucial technique in SPH formulations to mitigate shock discontinuities. Its primary function is to eliminate gaps between particles, thereby enhancing the simulation's resemblance to a continuous domain of fluid (Monaghan 1992).

In this study, we assess the effectiveness of two viscosity schemes. The first is a widely adopted approach proposed by Monaghan (1992), while the second involves a more sophisticated combination of laminar viscosity and sub-particle turbulence introduced by Dalrymple & Rogers (2006).

4.8.1 Using Artificial Viscosity

The outcomes of employing standard artificial viscosity are depicted in Figures 21 and 22. However, it is evident that the artificial viscosity scheme falls short in faithfully capturing the rheological properties of the fluid. Notably, it fails to adequately decelerate as the fluid flows, indicating a deviation from the experimental results.

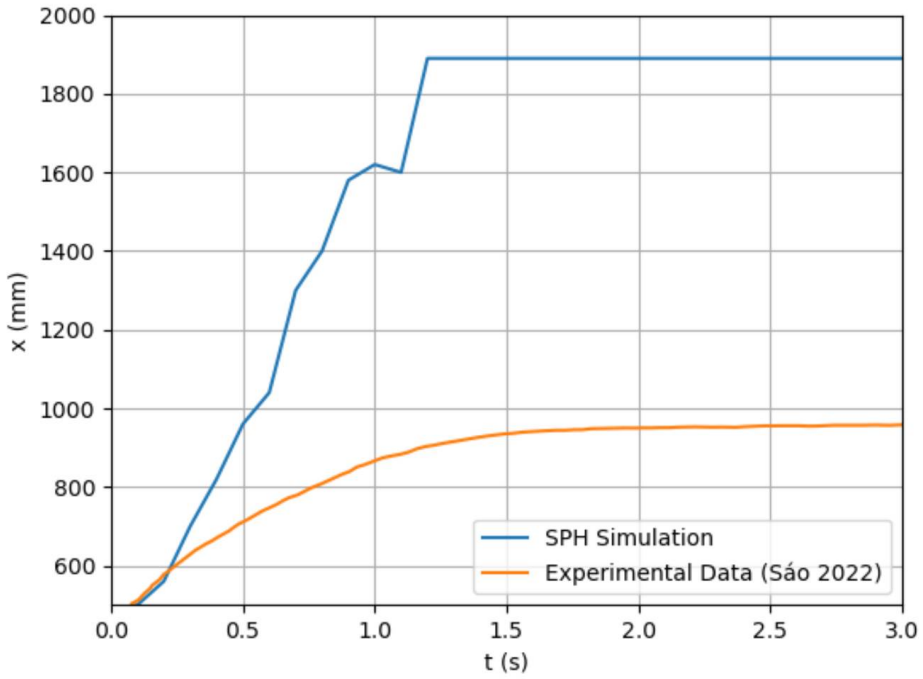

Figure 21: SPH Results for the Dambreak Wave Reach Throughout the Simulation Using Artificial Viscosity

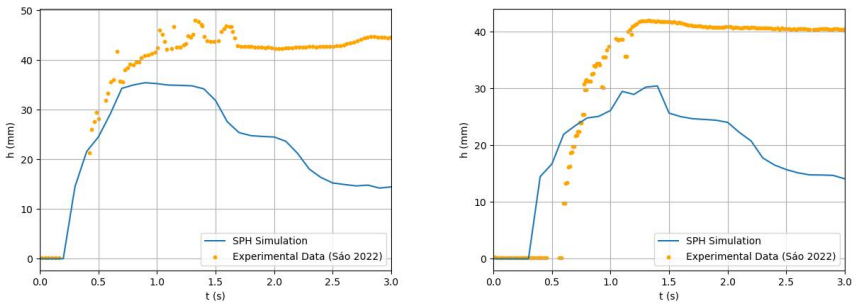

(a) Sensor1 (b) Sensor 2

Figure 22: SPH Results for Depth Below each Sensor Throughout the Simulation Using Artificial Viscosity

The artificial viscosity's employment's failure to capture the rheological properties is further enforced by the calculation of the relative errors, as shown in Figure 23 for the dambreak reach. The average relative error throughout the simulation was of

77% for the dambreak reach and of 39% and 64% for depth below the first and second sensors.

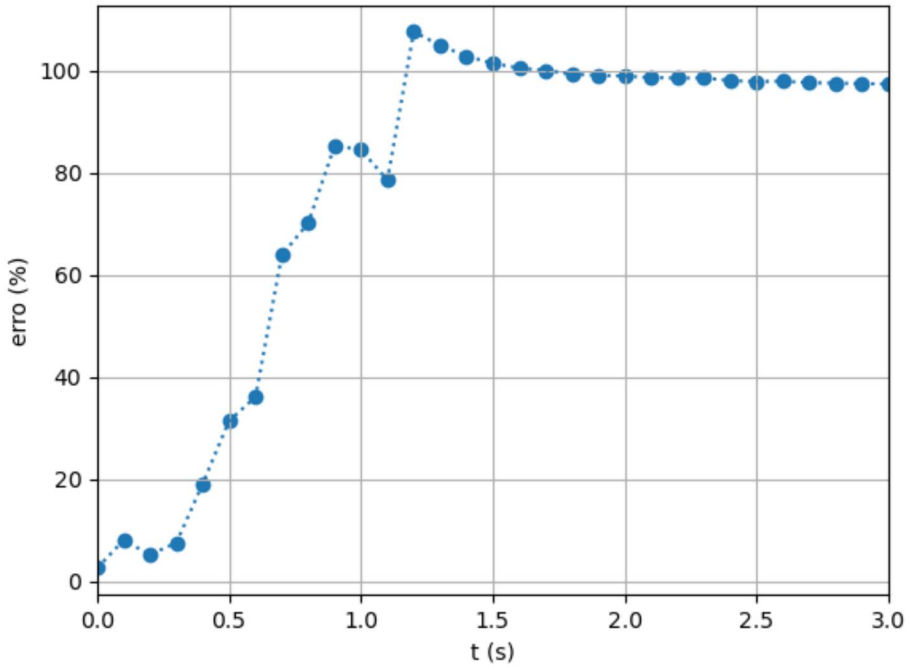

Figure 23: Relative Error Throughout the Simulation Using Artificial Viscosity

4.8.2 Laminar and sub particle turbulence

In contrast, the scheme employing laminar viscosity and sub-particle turbulence, showcased in Figures 24 and 25, more accurately reproduces the rheological properties of the fluid. The results exhibit a closer alignment with the experimental observations, emphasizing the effectiveness of this more sophisticated viscosity model.

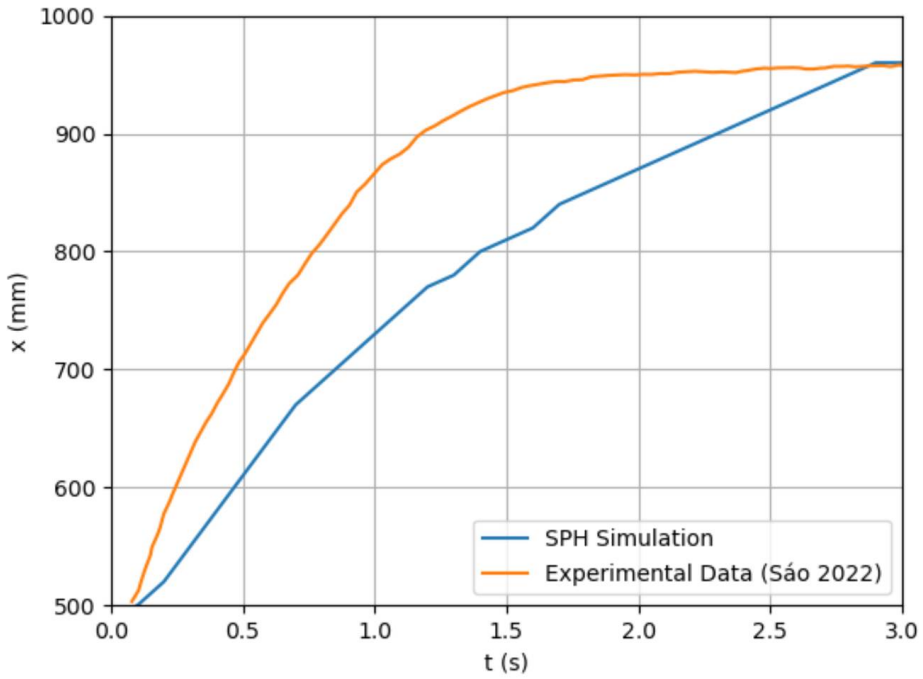

Figure 24: SPH Results for the Dambreak Wave Reach Throughout the Simulation Using Laminar and Sub Particle Turbulence

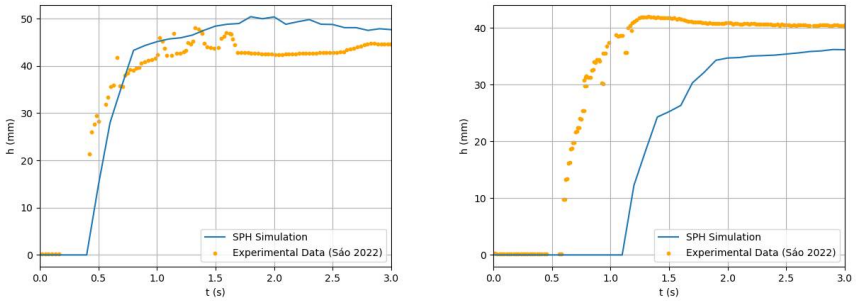

(a) Sensor1 (b) Sensor 2

Figure 25: SPH Results for Depth Below each Sensor Throughout the Simulation Using Laminar and Sub Particle Turbulence Viscosity

The relative error calculated for the simulation results using the laminar and sub-particle turbulence artificial viscosity scheme are shown in Figure 26. The average relative error was 10% for the reach and 12% and 23% for sensor 1 and 2, respectively.

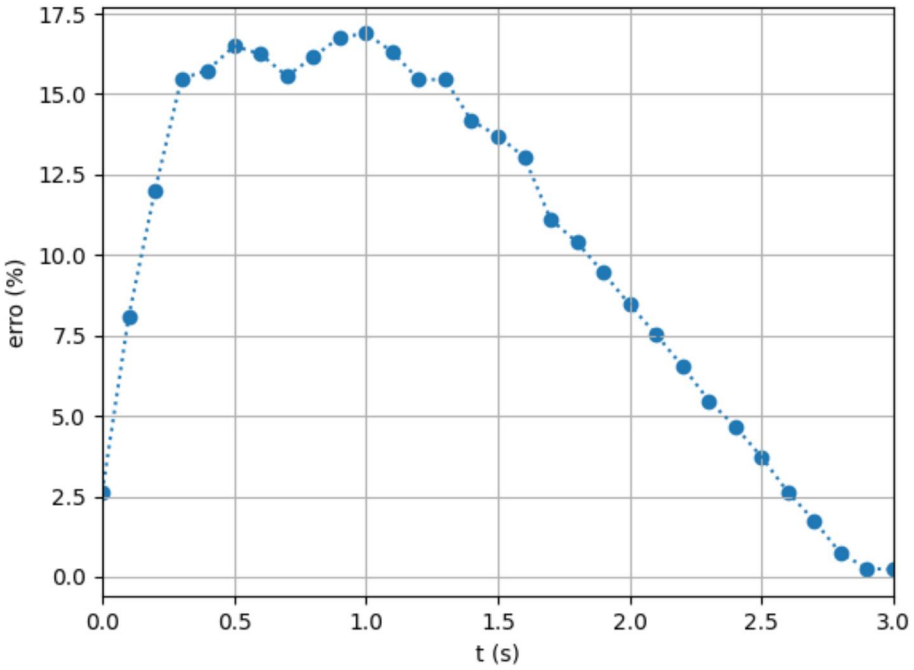

Figure 26: Relative Error Throughout the Simulation Using Laminar and Sub Particle Turbulence Viscosity

4.9 REMAINING SCENARIOS

Three options for artificial density diffusion and two choices for time-stepping schemes were considered with the lack of a clear best choice among the individual options, we opted for a comparison of all six possible combinations. This approach allowed us to delve deeper than individual evaluations and look for subtle improvements visible due to the combination of these parameters.

4.9.1 Time-Stepping

As with other computational fluid dynamics models, the time-stepping scheme plays a crucial role in maintaining stability and ensuring convergence of the Smoothed Particle Hydrodynamics model. While explicit solvers are popular due to their computational efficiency, they can be susceptible to instabilities.

As a first approach, we explored the Verlet time-stepping scheme introduced by Verlet (1967). Its popularity in particle dynamics stems from its computational efficiency, making it attractive for large SPH simulations. The Verlet scheme updates particle positions, velocities, and densities at each time step. However, due to the

decoupling of the density equation in SPH, an intermediate time-step is necessary for updating density before advancing positions and velocities. This additional step slightly increases the computational cost compared to a fully Verlet-compatible density update, but it maintains stability and accuracy in SPH simulations.

We also investigated a hybrid symplectic-Verlet time-stepping scheme. This approach combines the stability and energy-preserving properties of symplectic integration with the computational efficiency of the Verlet scheme for certain variables. This scheme follows the formulation of Leimkuhler & Matthews (2016), applying symplectic integration to update particle velocities and positions. Meanwhile, using the formulation proposed by Parshikov et al. (2000) for density calculations.

4.9.2 Density Diffusion

In an effort to mitigate density fluctuations and reduce noise caused by shocks and turbulent flows, Molteni & Colagrossi (2009) introduced the artificial density diffusion scheme. This approach evens out density values among neighboring particles, promoting a smoother density distribution throughout the computational domain.

Beyond the original formulation by Molteni & Colagrossi (2009), we test one other way to calculate the density diffusion and the model without density diffusion for comparison. The second formulation tested was proposed by Fourtakas et al. (2019) in a way to improve the behaviour of particle's density values close to boundaries.

5 RESULTS AND DISCUSSION

The results for the dambreak reach for combinations of the time stepping and density diffusion are shown in Figure 27 while the depth below the sensors are compared in Figure 28 for the first sensor, and in Figure 29 for the second one. By comparing the graphics for different combinations of setting we can see that there is no clear better opting amongst them.

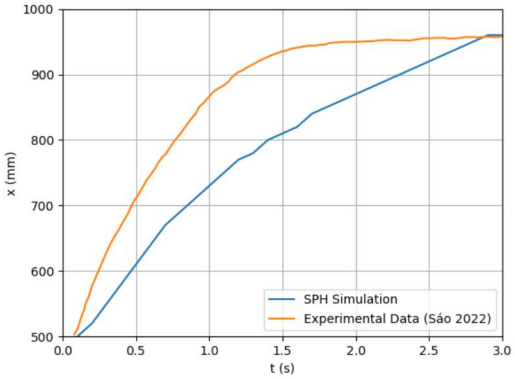

(a) Sympletic Time Stepping and No Density Diffusion

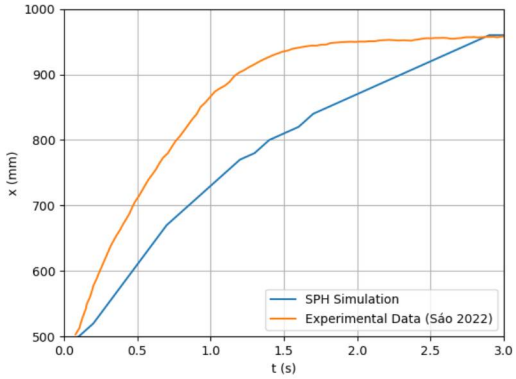

(b) Sympletic Time Stepping and Molteni Density Diffusion

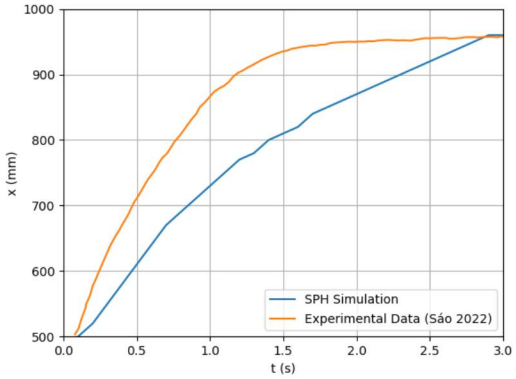

(c) Sympletic Time Stepping and Fourtakas Density Diffusion

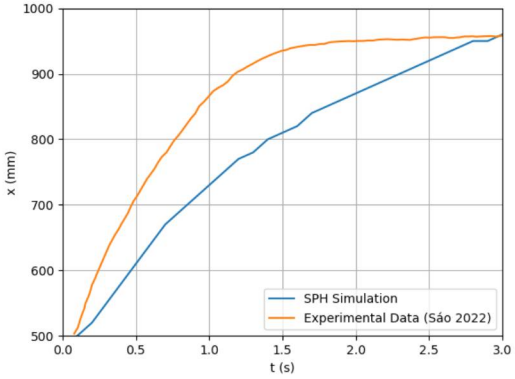

(d) Verlet Time Stepping and No Density Diffusion

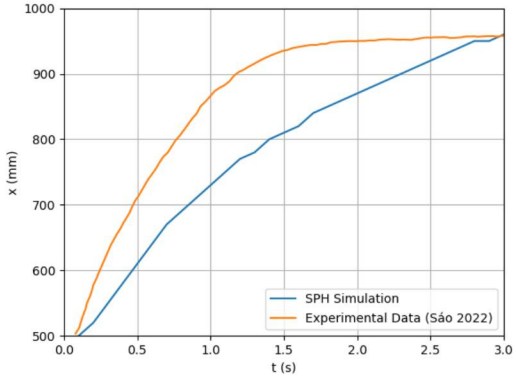

(e) Verlet Time Stepping and Molteni Density Diffusion

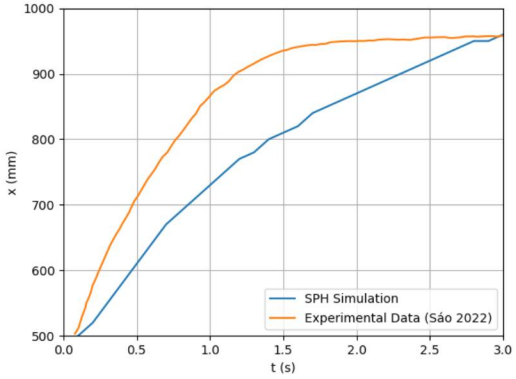

(f) Verlet Time Stepping and Fourtakas Density Diffusion

Figure 27: SPH Results for the Dambreak Wave Reach Throughout the Simulation For the Remaining Scenarios

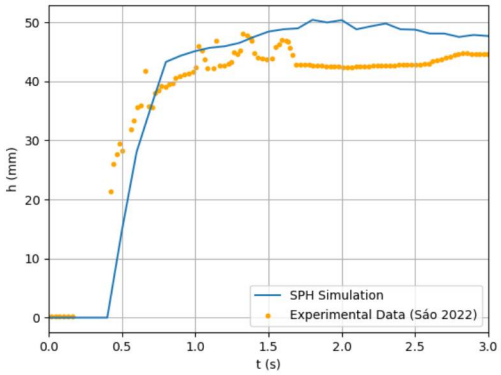

(a) Sympletic Time Stepping and No Density Diffusion

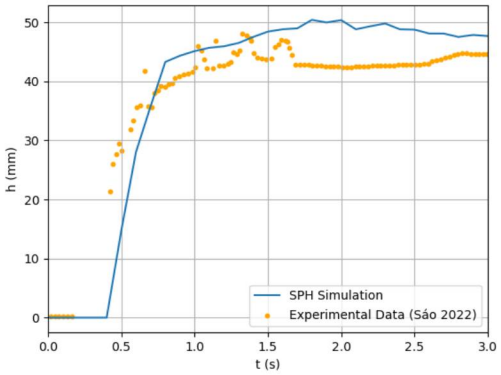

(b) Sympletic Time Stepping and Molteni Density Diffusion

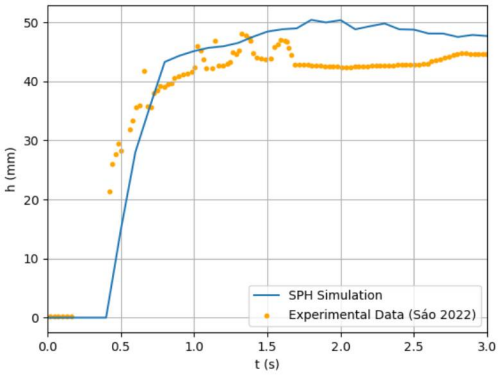

(c) Sympletic Time Stepping and Fourtakas Density Diffusion

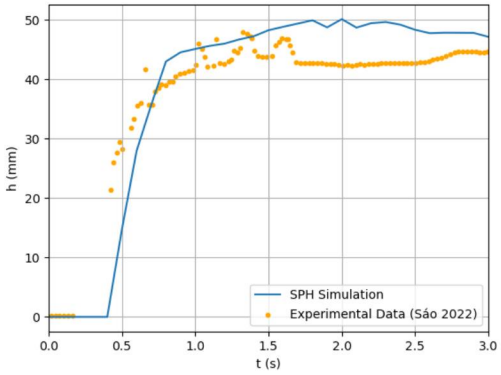

(d) Verlet Time Stepping and No Density Diffusion

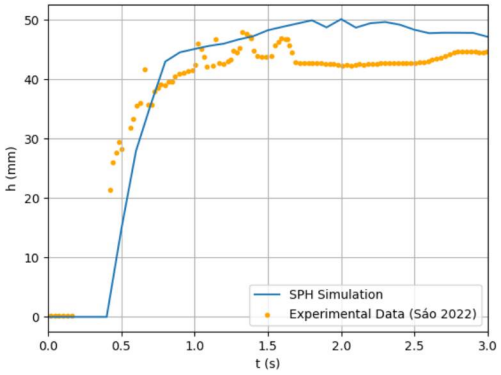

(e) Verlet Time Stepping and Molteni Density Diffusion

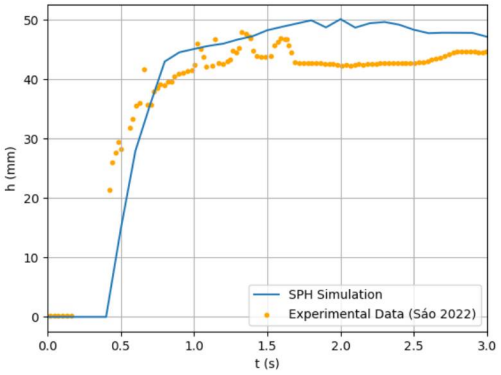

(f) Verlet Time Stepping and Fourtakas Density Diffusion

Figure 28: SPH Results for Depth Below the First Sensor Throughout the Simulation for The Remaining Scenarios

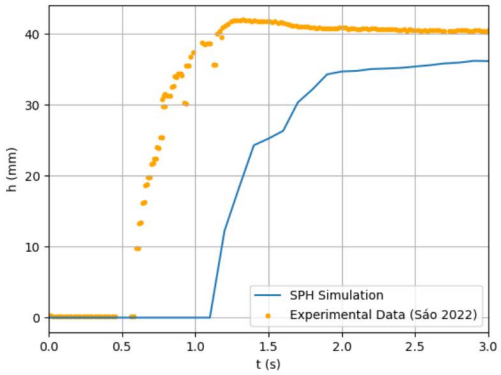

(a) Sympletic Time Stepping and No Density Diffusion

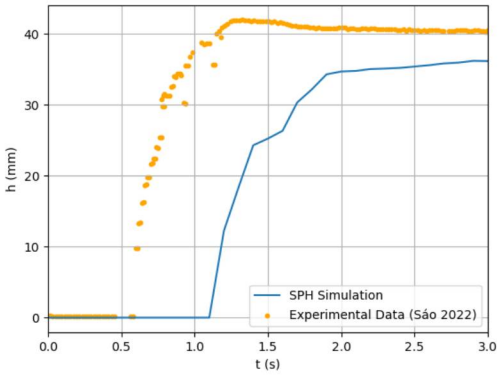

(b) Sympletic Time Stepping and Molteni Density Diffusion

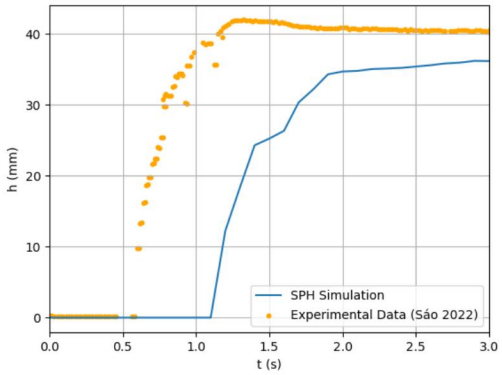

(c) Sympletic Time Stepping and Fourtakas Density Diffusion

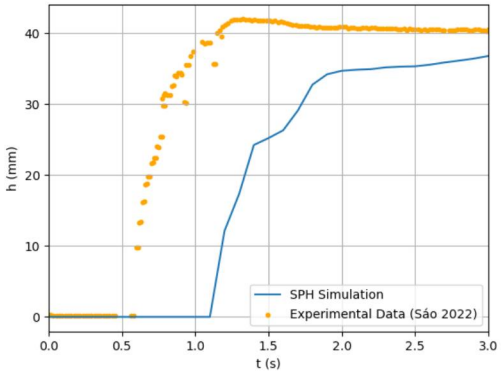

(d) Verlet Time Stepping and No Density Diffusion

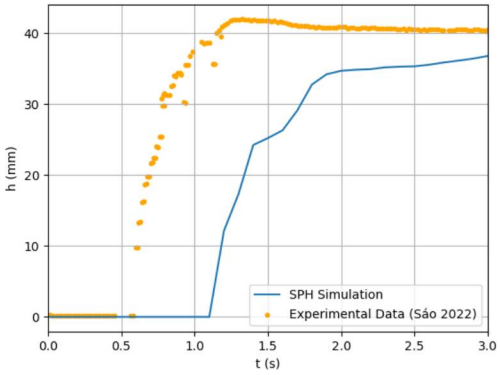

(e) Verlet Time Stepping and Molteni Density Diffusion

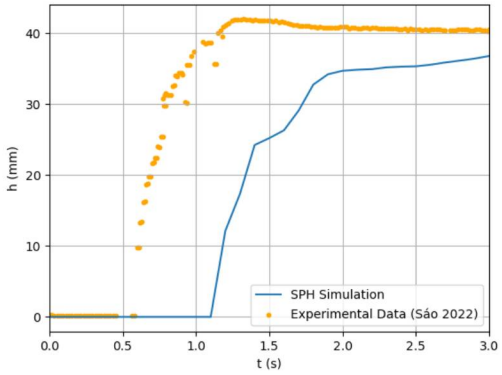

(f) Verlet Time Stepping and Fourtakas Density Diffusion

Figure 29: SPH Results for Depth Below the Second Sensor Throughout the Simulation for The Remaining Scenarios

By looking back at the settings compared, we can see how we got to the setting used to test the calibration parameter in the first place, since there were clear better options for many of the settings available and for the time-stepping and artificial density diffusion there was no clear better option.

By comparing the average relative error throughout the simulations, we can select a better option by a marginal difference. The density diffusion different methods don't result in any difference in the results, big enough density gradients don't occur during the dambreak simulations for the density diffusion to be meaningful. The marginal difference is seen by comparing the different time step schemes.

The Sympletic time-stepping average relative errors were of 10% for the dambreak wave reach, 12% for the depth below the first sensor and 24% for the depth below the second sensor. Meanwhile, the Verlet time-stepping average relative errors were of 10% for the dambreak wave reach, 12% for the depth below the first sensor and 23% for the depth below the second sensor. This means, using the Verlet time stepping had a better match to experimental data.

6 CONCLUSION

The adjusted non-Newtonian formulation appeared to closely mimic the behavior of the original Herschhel-Bulkley model. Since the objective was to help the lower deformation stages of the flow not to deal with too high apparent viscosities, the formulation used was proven suitable for its use.

Ultimately, we couldn't properly adjust the model simulation to fit the experimental data. While certain aspects exhibited agreement between the simulated and the measured, notably the middle-section of the dam-break flow and the fluid depth measured below both sensors, it wasn't enough to fit the entire simulated results to experimental data.

Since the majority of the disparity occurred in the early to middle parts of the simulation, the way the moving dam was implemented might be the source of the disparity. As previously mentioned, the boundary particles interact with the fluid particles by increasing density around them and preventing fluid particles from crossing. The gap they might form around that was accounted for during the boundary setup might not work properly around the moving dam, causing repulsion between boundary and fluid when there shouldn't be, especially below the dam while it rises. This may prevent the fluid from flowing when it should flow, during the first time steps, and constrain flow in a way it shouldn't, during the middle steps of the simulation. As the dam stops influencing the flow, it matches the experimental data better, in the

later stages of the simulation.

Because of this, we assume that, in order to accurately match the simulation results to the experimental data, it is necessary to fix the way the rising dam influences the flow. This could be done by changing the boundary properties, setting them up differently. One potential approach would be to implement the boundary conditions proposed by English et al. (2019), which involves incorporating ghost particles outside the domain and updating them during SPH particle updates, as suggested by Marrone et al. (2011).

References

Boger, David V. 2013. Rheology of slurries and environmental impacts in the mining industry. *Annual Review of Chemical and Biomolecular Engineering* 4(1). 239–257. doi: 10.1146/annurev-chembioeng-061312-103347.

Crespo, A. J. C., M. Gómez-Gesteira & R. A. Dalrymple. 2007. Boundary conditions generated by dynamic particles in SPH methods 5(3). 173–184. doi:https://doi.org/10.3970/cmc.2007.005.173.

Crespo, Alejandro C., Jose M. Dominguez, Anxo Barreiro, Moncho Gómez-Gesteira & Benedict D. Rogers. 2011. Gpus, a new tool of acceleration in cfd: Efficiency and reliability on smoothed particle hydrodynamics methods. *PLoS ONE* 6(6). e20685. doi:10.1371/journal.pone.0020685.

Dalrymple, R.A. & B.D. Rogers. 2006. Numerical modeling of water waves with the sph method. *Coastal Engineering* 53(2–3). 141–147. doi:10.1016/j.coastaleng.2005.10.004.

Dalrymple, Robert A. & Omar Knio. 2001. Sph modelling of water waves. In *Coastal dynamics '01*, American Society of Civil Engineers. doi:10.1061/40566(260)80.

Desbrun, Mathieu & Marie-Paule Gascuel. 1996. *Smoothed particles: A new paradigm for animating highly deformable bodies* 61–76. Springer Vienna. doi:10.1007/978-3-7091-7486-9_5.

Ding, Lijun & Ardeshir Goshtasby. 2001. On the canny edge detector. *Pattern Recognition* 34(3). 721–725. doi:10.1016/s0031-3203(00)00023-6.

Domínguez, J. M., G. Fourtakas, C. Altomare, R. B. Canelas, A. Tafuni, O. García-Feal, I. Martínez-Estévez, A. Mokos, R. Vacondio, A. J. C. Crespo, B. D. Rogers, P. K. Stansby & M. Gómez-Gesteira. 2021. DualSPHysics: from fluid dynamics to multiphysics problems. *Computational Particle Mechanics* 9(5). 867–895. doi: 10.1007/s40571-021-00404-2.

English, Aaron, José Domínguez, Renato Vacondio, Alejandro Crespo, P.K. Stansby, Steven Lind & Moncho Gesteira. 2019. Correction for dynamic boundary conditions, .

Fang, Xiang-Li, Fu-Ren Ming, Ping-Ping Wang, Peng-Nan Sun & A-Man Zhang. 2022. Application of sph method in the study of ship capsizing induced by large-scale rising bubble. *Ocean Engineering* 257. 111629. doi:10.1016/j.oceaneng.2022.111629.

Fourtakas, Georgios, Jose M. Dominguez, Renato Vacondio & Benedict D. Rogers. 2019. Local uniform stencil (lust) boundary condition for arbitrary 3-d boundaries in parallel smoothed particle hydrodynamics (sph) models. *Computers Fluids* 190. 346–361. doi:10.1016/j.compfluid.2019.06.009.

Frigaard, I.A. & C. Nouar. 2005. On the usage of viscosity regularisation methods for visco-plastic fluid flow computation. *Journal of Non-Newtonian Fluid Mechanics* 127(1). 1–26. doi:10.1016/j.jnnfm.2005.01.003.

Gingold, R. A. & J. J. Monaghan. 1977. Smoothed particle hydrodynamics: theory and application to non-spherical stars. *Monthly Notices of the Royal Astronomical Society* 181(3). 375–389. doi:10.1093/mnras/181.3.375.

Hérault, Alexis, Giuseppe Bilotta & Robert A. Dalrymple. 2010. SPH on GPU with CUDA. *Journal of Hydraulic Research* 48(sup1). 74–79. doi:10.1080/00221686.

2010.9641247.

Herschel, Winslow H. & Ronald Bulkley. 1926. Konsistenzmessungen von gummi-benzollösungen. *Kolloid-Zeitschrift* 39(4). 291–300. doi:10.1007/bf01432034.

Hosseini, S.M., M.T. Manzari & S.K. Hannani. 2007. A fully explicit three-step SPH algorithm for simulation of non-newtonian fluid flow. *International Journal of Numerical Methods for Heat &amp Fluid Flow* 17(7). 715–735. doi:10.1108/09615530710777976.

Hu, Liming, Hui Wu, Lin Zhang, Pengwei Zhang & Qingbo Wen. 2017. Geotechnical properties of mine tailings. *Journal of Materials in Civil Engineering* 29(2). doi:10.1061/(asce)mt.1943-5533.0001736.

Hu, X.Y. & N.A. Adams. 2006. A multi-phase sph method for macroscopic and mesoscopic flows. *Journal of Computational Physics* 213(2). 844–861. doi:10.1016/j.jcp.2005.09.001.

Jing, Xiaofei, Yulong Chen, Dan Xie, David J. Williams, Shangwei Wu, Wensong Wang & Tianwei Yin. 2019. The effect of grain size on the hydrodynamics of mudflow surge from a tailings dam-break. *Applied Sciences* 9(12). 2474. doi:10.3390/app9122474.

Kwak, Minkyung, David F. James & Katherine A. Klein. 2005. Flow behaviour of tailings paste for surface disposal. *International Journal of Mineral Processing* 77(3). 139–153. doi:10.1016/j.minpro.2005.06.001.

Leimkuhler, Benedict & Charles Matthews. 2016. Efficient molecular dynamics using geodesic integration and solvent–solute splitting. *Proceedings of the Royal Society A: Mathematical, Physical and Engineering Sciences* 472(2189). 20160138. doi:10.1098/rspa.2016.0138.

Liu, Shielan & Michael Henderson. 2020. An overview on methodologies for tailings dam breach study, .

Lo, Edmond Y.M. & Songdong Shao. 2002. Simulation of near-shore solitary wave mechanics by an incompressible SPH method. *Applied Ocean Research* 24(5). 275–286. doi:10.1016/s0141-1187(03)00002-6.

Marrone, S., M. Antuono, A. Colagrossi, G. Colicchio, D. Le Touzé & G. Graziani. 2011. []-sph model for simulating violent impact flows. *Computer Methods in Applied Mechanics and Engineering* 200(13–16). 1526–1542. doi:10.1016/j.cma.2010.12.016.

Molteni, Diego & Andrea Colagrossi. 2009. A simple procedure to improve the pressure evaluation in hydrodynamic context using the SPH. *Computer Physics Communications* 180(6). 861–872. doi:10.1016/j.cpc.2008.12.004.

Monaghan, J. J. 1982. Why particle methods work. *SIAM Journal on Scientific and Statistical Computing* 3(4). 422–433. doi:10.1137/0903027.

Monaghan, J. J. 1992. Smoothed particle hydrodynamics. *Annual Review of Astronomy and Astrophysics* 30(1). 543–574. doi:10.1146/annurev.aa.30.090192.002551.

Monaghan, J. J., R. A. F. Cas, A. M. Kos & M. Hallworth. 1999. Gravity currents descending a ramp in a stratified tank. *Journal of Fluid Mechanics* 379. 39–69. doi:10.1017/s0022112098003280.

Monaghan, J. J. & J. C. Lattanzio. 1985. A refined particle method for astrophysical problems. *Astronomy and Astrophysics* 149(1). 135–143.

Moon, N, M Parker, HJJ Boshoff & D Clohan. 2019. Advances in non-newtonian

dam break studies 15.

O'Brien, J. S., P. Y. Julien & W. T. Fullerton. 1993. Two-dimensional water flood and mudflow simulation. *Journal of Hydraulic Engineering* 119(2). 244–261. doi: 10.1061/(asce)0733-9429(1993)119:2(244).

Owens, J.D., M. Houston, D. Luebke, S. Green, J.E. Stone & J.C. Phillips. 2008. Gpu computing. *Proceedings of the IEEE* 96(5). 879–899. doi:10.1109/jproc.2008.917757.

de Paiva, Camilla Adriane, Aníbal da Fonseca Santiago & José Francisco do Prado Filho. 2020. Content analysis of dam break studies for tailings dams with high damage potential in the quadrilátero ferrífero, minas gerais: technical weaknesses and proposals for improvements. *Natural Hazards* 104(2). 1141–1156. doi:10.1007/s11069-020-04254-8.

Papanastasiou, Tasos C. 1987. Flows of materials with yield. *Journal of Rheology* 31(5). 385–404. doi:10.1122/1.549926.

Parshikov, Anatoly N., Stanislav A. Medin, Igor I. Loukashenko & Valery A. Milekhin. 2000. Improvements in SPH method by means of interparticle contact algorithm and analysis of perforation tests at moderate projectile velocities. *International Journal of Impact Engineering* 24(8). 779–796. doi:https://doi.org/10.1016/S0734-743X(99)00168-2.

Pereira, João Batista. 2018. *Desenvolvimento de aparato automatizado de slump test: Ferramenta de controle de qualidade e de caracterização reológica de materiais.* Universidade Estadual Paulista "Júlio De Mesquita Filho" MA thesis.

Quinlan, N. J., M. Basa & M. Lastiwka. 2006. Truncation error in mesh□free particle methods. *International Journal for Numerical Methods in Engineering* 66(13). 2064–2085. doi:10.1002/nme.1617.

Shao, J.R., H.Q. Li, G.R. Liu & M.B. Liu. 2012. An improved sph method for modeling liquid sloshing dynamics. *Computers amp; Structures* 100–101. 18–26. doi:10.1016/j.compstruc.2012.02.005.

Shao, Songdong & Edmond Y.M. Lo. 2003. Incompressible SPH method for simulating newtonian and non-newtonian flows with a free surface. *Advances in Water Resources* 26(7). 787–800. doi:10.1016/s0309-1708(03)00030-7.

Sáo, Yuri Taglieri. 2021. *Investigação numérico-experimental da influência de efeitos de inércia em escoamentos de fluidos viscoplásticos modelados como ruptura de barragem.* Universidade Estadual Paulista "Júlio De Mesquita Filho" MA thesis.

Wendland, Holger. 1995. Piecewise polynomial, positive definite and compactly supported radial functions of minimal degree. *Advances in Computational Mathematics* 4(1). 389–396. doi:10.1007/bf02123482.